Standing-Wave Oscillations in Binary Mixture Convection: From the Onset via Symmetry Breaking to Period Doubling into Chaos

P. Matura, D. Jung, and M. Lücke

Institut für Theoretische Physik, Universität des Saarlandes, D-66041 Saarbrücken, Germany

(Received 18 November 2003; published 25 June 2004)

Oscillatory solution branches of the hydrodynamic field equations describing convection in the form of a standing wave (SW) in binary fluid mixtures heated from below are determined completely for several negative Soret coefficients ψ. Galerkin as well as finite-difference simulations were used. They were augmented by simple control methods to obtain also unstable SW states. For sufficiently negative ψ, unstable SWs bifurcate subcritically out of the quiescent conductive state. They become stable via a saddle-node bifurcation when lateral phase pinning is exerted. Eventually their invariance under timeshift by half a period combined with reflection at midheight of the fluid layer gets broken. Thereafter, they terminate by undergoing a period-doubling cascade into chaos.

DOI: 10.1103/PhysRevLett.92.254501 PACS numbers: 47.20.Ky, 05.45.–a, 47.54.+r

Convection in one-component fluids such as pure water occurs in Rayleigh-Bénard setups of narrow channels heated from below in the form of stationary rolls. However, adding, for instance, 5% of ethanol to the water, the spatiotemporal behavior of the possible convective structures becomes much richer [1]. The reason is that concentration variations which are generated via the Soret effect by externally imposed and by internal temperature gradients influence the buoyancy, i.e., the driving force for convective flow. The latter in turn mixes by advectively redistributing concentration. This nonlinear advection gets in developed convective flow typically much larger than the smoothening by linear diffusion—Péclet numbers measuring the strength of advective concentration transport relative to diffusion are easily of the order of a thousand. Thus, the concentration balance is strongly nonlinear giving rise to strong variations of the concentration field and to boundary layer behavior as in Fig. 1. In contrast to that, momentum and heat balances remain weakly nonlinear close to onset as in pure fluids implying only smooth and basically harmonic variations of velocity and temperature fields as of the critical modes, cf. Fig. 1. Hence, the feedback interplay between (i) the Soret generated concentration variations, (ii) the resulting modified buoyancy, and (iii) the strongly nonlinear advective transport and mixing causes binary mixture convection to be rather complex with respect to its spatiotemporal properties and its bifurcation behavior.

Take, for example, the case of negative Soret coupling, $\psi < 0$, between deviations δT and δC of temperature and concentration, respectively, from their means [4]. Then the above described feedback interplay generates oscillations. They show up in transient growth of convection [3] at supercritical heating, in relaxed nonlinear traveling wave (TW) and standing wave (SW) solutions that branch subcritically out of the conductive state via a common Hopf bifurcation, and in spatially localized traveling wave (LTW) states. TW and LTW convection has been studied experimentally and theoretically in detail [1,5–13]. But little is known about nonlinear SW states beyond a weakly nonlinear analysis [14] that is restricted to the immediate vicinity of the oscillatory threshold. It showed that SWs are unstable there, typically bifurcating backwards.

Here we determine for the first time structure, dynamics, and bifurcation behavior of SWs for several ψ. We stabilize the unstable SWs by control methods which can similarly also be applied in experiments. We found that they undergo a period-doubling cascade into chaos after a symmetry has been broken that relates upflow and downflow to each other.

Calculations were done for mixtures such as ethanol water for Lewis number $L = 0.01$ and Prandtl number $\sigma = 10$. The field equations were solved in a vertical cross section through the convection rolls perpendicular to their axes. A multimode Galerkin method as well as a finite-difference method were used showing agreement with each other. Horizontal boundaries at top and bottom, $z = \pm 1/2$, were no slip, perfectly heat conducting, and impermeable. Laterally, we impose periodic boundary conditions with wave number $k = \pi$. In addition, we suppress phase propagation. We stabilize the SW states by exerting control via the field amplitudes (or the heat current injected into the fluid) and the Rayleigh number R in response to the instantaneous frequency and its temporal derivative, respectively [15]. In this way we trace out the SW solution branch all the way from close to onset with large frequency to slowly oscillating SWs that eventually period double into chaos. The procedure starts from a supercritically growing transient SW with subsequent reduction of the heating below threshold.

We use $r = R/R_c^0$ to measure the thermal driving. $R_c^0 = 1707.762$ is the critical Rayleigh number for onset of convection in a pure fluid. The flow induced mixing is measured by the mixing number $M(t)$ that is defined in terms of the mean square concentration deviation, $M^2 = \langle(\delta C)^2\rangle/\langle(\delta C_{\mathrm{cond}})^2\rangle$. Here, the brackets denote spatial averaging. In a perfectly mixed fluid, M vanishes

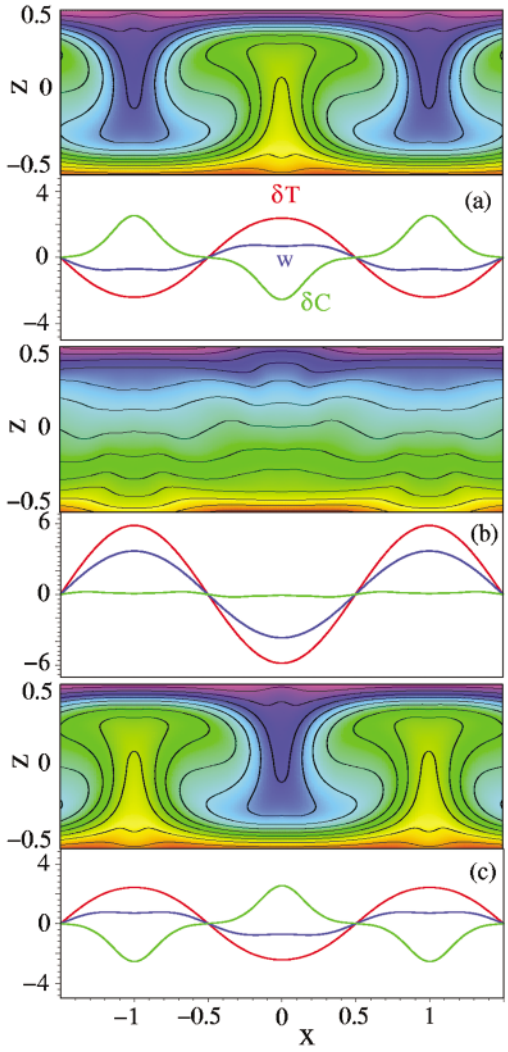

FIG. 1 (color). Snapshots of SW convection for $r = 1.15$, $\psi = -0.25$ during half of its oscillation period $\tau = 2\pi/\omega = 1.4$. The concentration distribution in the vertical cross section through the layer is color coded with blue and red denoting high and low concentration, respectively. Lateral wave profiles of vertical velocity w, temperature δT, and concentration δC at midheight, $z = 0$, are shown by colored lines: w, blue; $40\delta T/R$, red; and $80\delta C/R$, green, respectively. At the snapshot times $t = 0$ (a), 0.265τ (b), and $\tau/2$ (c) $\delta C(x = 0, z = 0, t)$ has a minimum, a zero crossing, and a maximum, respectively. This SW shows the MTS explained in the text.

while $M = 1$ in the conductive state (denoted by the subscript cond) with its large Soret-induced vertical concentration gradient.

In Fig. 1, we show snapshots of SW convection in order to display characteristic symmetry and structural properties. SWs are laterally mirror symmetric around positions of maximal upflow and downflow; e.g., $x = 0$ and the node locations of the fields are fixed in time. Furthermore, all fields have at every instant definite parity under the mirror-glide operation $(x, z) \rightarrow (x + \lambda/2, -z)$ of vertical reflection at midheight, $z = 0$, combined with lateral translation by half a wavelength. We did not observe SWs without this symmetry—perturbations breaking it that we introduced for test purposes always decayed rapidly to zero. Finally, the fields of Fig. 1 have a definite mirror-timeshift symmetry (MTS); e.g., $f(x, z, t) = -f(x, -z, t + \tau/2)$ for $f = \delta C, \delta T$, and the vertical velocity field w with $\tau = 2\pi/\omega$ being the SW oscillation period. At midheight, the condition $f(t) = -f(t + \tau/2)$ implies, in particular, that positive and negative field extrema of an oscillation cycle have equal magnitudes. SWs with smaller frequency break this symmetry which is a prerequisite for period doubling [16].

Since the concentration balance is dominated by nonlinear advection, the distribution of δC (color coded plots in Fig. 1) shows plumelike structures and narrow boundary layers. Consequently, the field profiles of δC which are shown in Fig. 1 at $z = 0$ are anharmonic. Also, the temporal oscillation of δC at a fixed location is anharmonic. On the other hand, temporal and spatial variations of w and δT are much smoother and almost harmonic. The oscillation of w is temporally delayed relative to that of δC: The latter being advected almost passively by the former changes the buoyancy driving force for w. At midheight, this phase shift increases from about 0.52π at onset to about 0.73π before the MTS breaks.

Figure 2 shows how the bifurcation behavior of SWs changes with Soret coupling strength $-0.4 \leq \psi \leq -0.03$. The solution branch for stationary overturning convection (SOC), which has the same spatial symmetries as SWs, is included for comparison only for $\psi = -0.03$. The heating range in which SWs exist increases when ψ becomes more negative since the oscillatory bifurcation threshold r_{osc} is shifted stronger to higher r than the SW saddle node at r_s^{SW} which marks the lower end of the r interval containing SWs. All these SWs bifurcate subcritically out of the conductive state as unstable solutions. They become stable via saddle-node bifurcations. However, when the phase-pinning condition is lifted completely then SWs decay by developing TW transients since any spatial phase difference between δC and w causes the extrema of the latter to be "pulled" towards the solutally shifted buoyancy extrema. Depending on r, these transients either end in a nonlinear TW or SOC or the conductive state.

Moving along an SW branch, the maximal vertical upflow velocity w_{max} [Fig. 2(a)] does not increase monotonically as in TWs and SOCs but rather has a maximum somewhat below the respective SOC value before it drops again. On the other hand, ω and M decrease monotonically starting with the Hopf frequency ω_{H} and $M = 1$, respectively, at onset. M and ω are related to each other almost linearly as in TWs [2].

The blowup of the lower part of Fig. 2(b) in Fig. 2(c) shows how stability and shape of the solution branches change with ψ. While the SW at $\psi = -0.03$ has only one saddle node, the curvature of the branches changes with decreasing ψ such that two additional saddle nodes arise

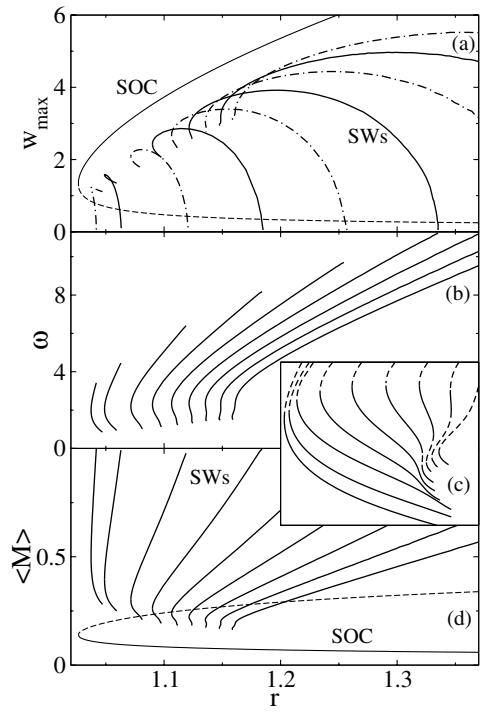

FIG. 2. Bifurcation properties of SWs for $\psi = -0.03, -0.05, -0.1, -0.15, -0.2, -0.25, -0.3, -0.35$, and -0.4 (from left to right): (a) Maximal vertical velocity w_{max}. (b) Frequency ω. (d) Time average of the mixing number M. The inset (c) shows a blowup of the lower part of (b), however, with shifted solution branches to better display their structural evolution with ψ. Full (dashed) lines in (c) identify stable (unstable) SWs. Unstable SWs bifurcate subcritically out of the quiescent conductive state [lower ends of the curves in (a); upper ends in (b) and (c)] and undergo stability changes via saddle-node bifurcations. The SOC solution branch is shown for the sake of clarity only for $\psi = -0.03$. SOC curves for the other ψ are shifted slightly to the right.

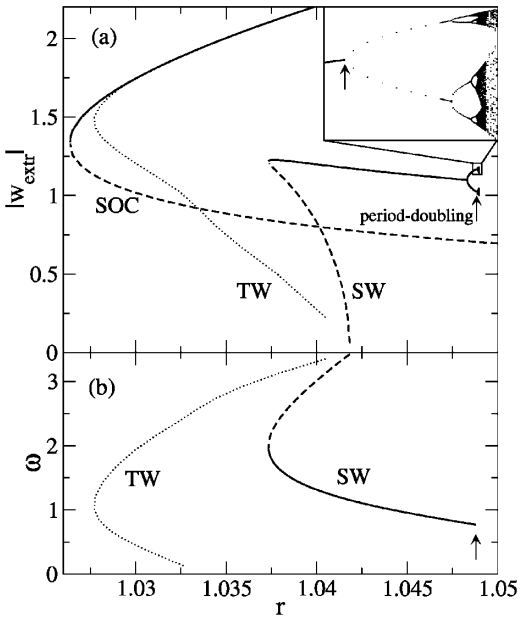

FIG. 3. Details of the bifurcation behavior for $\psi = -0.03$ (leftmost curves in Fig. 2). (a) Magnitude $|w_{extr}|$ of the extrema in the vertical flow. (b) Frequency ω. For the sake of completeness, we include also the TW solution for laterally periodic boundary conditions allowing free phase propagation. SW and TW bifurcate subcritically at $r_{osc} = 1.0418$ with Hopf frequency $\omega_H = 3.426$. The TW branch ends by merging with zero frequency with the SOC solution branch. The SW solution becomes stable (solid lines) at the saddle-node position $r_s^{SW} = 1.0373$. At $r = 1.048\,31$, the MTS is broken and the solid SW line in (a) splits into two when the magnitudes of the vertical flow extrema occurring during one oscillation cycle become different [see, e.g., Fig. 4(b) where the downflow at $x = 0 = z$ is more intense than the upflow]. This MTS-broken SW starts to undergo at $r = 1.048\,83$ (marked by arrows) a period-doubling route to chaos that is shown in more detail in the inset of (a).

(for $\psi = -0.25, -0.3, -0.35$) with associated stability changes. For $\psi = -0.4$, we have only one saddle node again.

The bifurcation behavior of the leftmost curves of Fig. 2 is displayed in more detail in Fig. 3. For the sake of completeness, the TW solution is shown as well. However, when phase propagation is suppressed as in our case, then the TW does not exist and the upper SOC solution branch [full line in Fig. 3(a)] is stable down to its saddle node.

Also the SW becomes stable via a saddle-node bifurcation. With increasing r, the flow amplitude of the stable SW (full lines) slightly decreases. Then the MTS breaks and the solution branch splits into two. Thereafter the downflow (upflow) extrema occurring in the SW oscillations, say, at $x = 0$ ($\pm \lambda/2$), are more intense than the upflow (downflow) extrema. Consequently, the time averaged fields have now a net SOC-like structure with nonzero mean downflow (upflow), say, at $x = 0$ ($\pm \lambda/2$).

Figure 4 shows the local dynamics of w and δC at $x = 0 = z$ and the global mixing number M before (left column) and after (right column) MTS breaking. By definition, M oscillates with twice the SW frequency as long as MTS holds. Note that, in particular, δC displays the characteristics of a relaxational oscillator. In the MTS-broken SW of Fig. 4, the extrema of upflow and downflow at $x = 0$ differ. Also the upflow and downflow times between the respective zero crossings of w differ.

In Fig. 5, we show how MTS breaking and period doubling changes the SW phase dynamics using w, $\dot{w}$, and M as characteristic local and global quantities, respectively. The particular MTS-broken SW orbits of Fig. 5 move closer to the SOC fixed point with downflow at $x = 0$. Here it would be interesting to see whether and how the heteroclinic orbits connecting the two unstable symmetry degenerate SOC fixed points organize and restrain the dynamics of the SWs that periodically switch between upflow and downflow.

For the ψ range considered here, we found that slightly after the MTS breaking a period-doubling scenario into chaos starts that is compatible within our numerical resolution with the Feigenbaum constant. For stronger

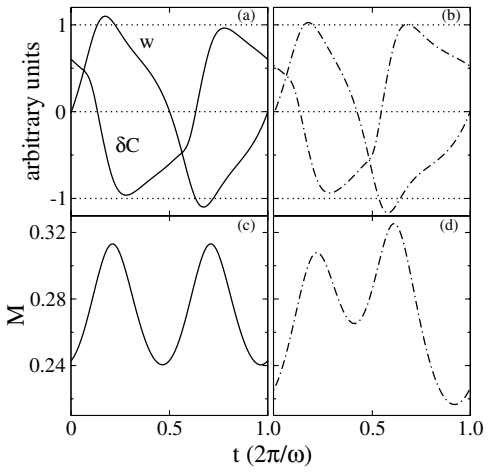

FIG. 4. Effect of MTS breaking on temporal oscillation profiles. Right (left) column shows a period-1 SW for $\psi = -0.03$ at $r = 1.0488$ (1.0483) where the MTS is (not yet) broken. Here w and δC are evaluated at midheight between two rolls, $x = 0 = z$. The mixing number M oscillates with twice the SW frequency as long as the MTS holds (c).

Soret coupling, e.g., $\psi = -0.25$, we could resolve also a r window with period-3 SW states and subsequent period doubling. However, we did not observe SWs beyond the chaotic window(s) seen, e.g., in the inset of Fig. 3(a). After increasing the heating beyond this threshold, the SWs developed transients into a stable SOC state with large convection amplitude [full line in Fig. 3(a)].

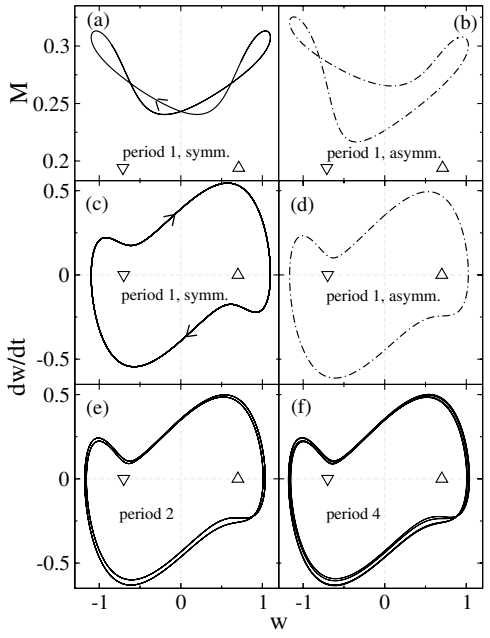

FIG. 5. MTS breaking and period doubling in the phase space dynamics of SWs. Shown are the mixing number M and $\dot{w}$ versus the vertical velocity w at $x = 0 = z$. In (a)–(d) the dash-dotted (full) lines refer to the period-1 SW in the right (left) column of Fig. 4 for which the MTS is (not yet) broken. Period doubling is displayed in (d)–(f). Upwards and downwards pointing triangles indicate symmetry degenerate unstable SOC fixed points (dashed SOC branches in Figs. 2 and 3) with upflow or downflow, respectively, at $x = 0$.

In summary, we have determined SW states in mixtures for several Soret coupling strengths. Close to onset of convection, the subcritical solutions are unstable. Under phase-pinning conditions, they become stable via saddle-node bifurcations. After the occurrence of a MTS breaking, they undergo a period-doubling cascade into chaos thereby terminating.

[1] M. C. Cross and P. C. Hohenberg, Rev. Mod. Phys. **65**, 851 (1993); and references, e.g., in [2,3].

[2] M. Lücke, W. Barten, P. Büchel, C. Fütterer, St. Hollinger, and Ch. Jung, in *Evolution of Spontaneous Structures in Dissipative Continuous Systems*, edited by F. H. Busse and S. C. Müller, Lecture Notes in Physics, Vol. M55 (Springer-Verlag, Berlin, 1998), p. 127.

[3] C. Fütterer and M. Lücke, Phys. Rev. E **65**, 036315 (2002).

[4] For 5 wt % of ethanol mixed into water at $T = 20\,^{\circ}\mathrm{C}$, the separation ratio measuring the Soret coupling strength is $\psi \simeq -0.3$.

[5] R. Heinrichs, G. Ahlers, and D. S. Cannell, Phys. Rev. A **35**, 2761 (1987); K. Lerman, D. S. Cannell, and G. Ahlers, Phys. Rev. E **59**, 2975 (1999).

[6] K. E. Anderson and R. P. Behringer, Physica (Amsterdam) **51D**, 444 (1991).

[7] B. L. Winkler and P. Kolodner, J. Fluid Mech. **240**, 31 (1992); P. Kolodner, Phys. Rev. E **50**, 2731 (1994).

[8] H. Touiri, J. K. Platten, and G. Chavepeyer, Eur. J. Mech. B **15**, 241 (1996).

[9] E. Moses, J. Fineberg, and V. Steinberg, Phys. Rev. A **35**, 2757 (1987); E. Kaplan, E. Kuznetsov, and V. Steinberg, Phys. Rev. E **50**, 3712 (1994).

[10] C. M. Surko, D. R. Ohlsen, S. Y. Yamamoto, and P. Kolodner, Phys. Rev. A **43**, 7101 (1991); C. M. Aegerter and C. M. Surko, Phys. Rev. E **63**, 46301 (2001).

[11] L. Z. Ning, Y. Harada, and H. Yahata, Prog. Theor. Phys. **98**, 551 (1997).

[12] O. Batiste, E. Knobloch, I. Mercader, and M. Net, Phys. Rev. E **65**, 016303 (2001).

[13] D. Jung and M. Lücke, Phys. Rev. Lett. **89**, 054502 (2002).

[14] W. Schöpf and W. Zimmermann, Phys. Rev. E **47**, 1739 (1993).

[15] We drive the system towards the unstable limit cycle (ULC) with frequency ω_* that is located on the subcritical SW solution branch as follows: To reduce deviations with growing (decreasing) convection amplitude A that decrease (increase) ω at fixed R, we set $A_{n+1} = A_n[1 + W_A(\omega - \omega_*)]$. Furthermore, when $\Delta\omega/\Delta t$ is negative (positive), we move towards the SW solution branch by decreasing (increasing) R according to $R_{n+1} = R_n(1 + W_R\Delta\omega/\Delta t)$. The control depends on the actual values of $\omega - \omega_*$ and $\Delta\omega/\Delta t$ and vanishes only at the ULC with the preselected frequency ω_*. The optimal weight factors W_A and W_R depend on ω_*.

[16] J. W. Swift and K. Wiesenfeld, Phys. Rev. Lett. **52**, 705 (1984).